H3K4me3 recognition by the COMPASS complex facilitates the restoration of this histone mark following DNA replication

Albert Serra-Cardona[1]†‡, Shoufu Duan[1]†, Chuanhe Yu[2], Zhiguo Zhang[1]*

During DNA replication, parental H3-H4 marked by H3K4me3 are transferred almost equally onto leading and lagging strands of DNA replication forks. Mutations in replicative helicase subunit, Mcm2 (Mcm2-3A), and leading strand DNA polymerase subunit, Dpb3 (*dpb3Δ*), result in asymmetric distributions of H3K4me3 at replicating DNA strands immediately following DNA replication. Here, we show that *mcm2-3A* and *dpb3Δ* mutant cells markedly reduce the asymmetric distribution of H3K4me3 during cell cycle progression before mitosis. Furthermore, the restoration of a more symmetric distribution of H3K4me3 at replicating DNA strands in these mutant cells is driven by methylating nucleosomes without H3K4me3 by the H3K4 methyltransferase complex, COMPASS. Last, both gene transcription machinery and the binding of parental H3K4me3 by Spp1 subunit of the COMPASS complex help recruit the enzyme to chromatin for the restoration of the H3K4me3-marked state following DNA replication, shedding light on inheritance of this mark following DNA replication.

INTRODUCTION

Eukaryotic DNA is packaged into chromatin, which regulates all DNA-related processes such as transcription, replication, or repair (*1–3*). The nucleosome, the basic repeating unit of chromatin, is composed of two histone H2A-H2B dimers and one H3-H4 tetramer wrapped by 147 base pairs (bp) of DNA. Histone posttranslational modifications (PTMs), such as methylation, acetylation, or phosphorylation, play an important role in the establishment and maintenance of chromatin states (*4, 5*). Moreover, perturbations in the epigenetic information encoded in nucleosomes can lead to tumorigenesis (*6*). Therefore, the preservation of histone PTMs and their transmission to the next generation of cells are crucial and yet elusive cellular processes.

DNA replication–coupled nucleosome assembly plays a critical role in the maintenance of chromatin states following DNA replication (*1, 4*). DNA replication initiates from DNA replication origins followed by continued DNA synthesis of leading strand and discontinued synthesis of lagging strands (Okazaki fragments) (*7*). Before DNA synthesis, nucleosomes ahead of DNA replication forks are temporarily disassembled to allow the DNA replication machinery to replicate nucleosomal DNA (*1, 8*). Immediately following DNA replication, replicated DNA is assembled into nucleosomes using both parental histones and newly synthesized histones, which contain modifications distinct from those in parental histones. Moreover, parental and new H3-H4 tetramers form distinct nucleosomes following DNA replication (*9*). A parental H3-H4 tetramer, which could, in principle, be transferred either to leading or lagging strands of DNA replication forks, can memorize its position along DNA during mitotic cell division (*10, 11*). Once assembled into nucleosomes using both parental and new H3-H4 tetramers, a "read and write" mechanism plays an important role in the restoration of

repressive histone marks, including H3K9me3 or H3K27me3 (*12–14*). The essence of this mechanism is that the recognition of H3K9me3 or H3K27me3 on nucleosomes with parental H3-H4 by its cognate modifying enzyme helps direct the enzyme to modify neighboring nucleosomes containing newly synthesized H3-H4. However, it remains in debate whether this mechanism also applies to active histone marks such as H3K4me3 (*15–17*).

In both yeast and mammalian cells, parental H3-H4 tetramers are almost symmetrically distributed onto leading and lagging strands of DNA replication forks (*18, 19*). In contrast, asymmetric distribution of parental H3-H4 proteins at leading and lagging strands detected in cells that will undergo asymmetric cell division is transmitted into two daughter cells with distinct properties (*20*). Recently, we and others found two pathways involved in the transfer of parental histone H3-H4 to leading and lagging strands of DNA replication forks (*18, 19, 21, 22*). The Mcm2-Ctf4-Polα axis facilitates the transfer of parental H3-H4 tetramers onto lagging strands of DNA replication forks (*21*). Mcm2, a subunit of the replicative helicase CMG, contains a histone-binding motif (HBM) (*23*). Mutations at the HBM that impair the interaction between Mcm2 and H3-H4 compromise the transfer of parental H3-H4, marked by H3K4me3, to lagging strands, resulting in a marked enrichment of H3K4me3 at leading strands compared to lagging strands during early S phase of the cell cycle. In contrast, mutations at Dpb3 and Dpb4, two subunits of leading strand DNA polymerase, Polε, lead to defects in the transfer of parental histones to leading strands and thereby an enrichment of H3K4me3 at lagging strands in *dpb3Δ* or *dpb4Δ* cells (*18*). However, it is not clear whether this asymmetric distribution of H3K4me3 is maintained during cell cycle progression and then transmitted into daughter cells during mitotic cell divisions. To address these questions, we analyzed the distribution of H3K4me3 at replicating DNA strands during cell cycle progression. We found that the asymmetry of H3K4me3-marked parental histones decreases in both *mcm2-3A* and *dpb3Δ* cells, with this mark reaching similar levels between leading and lagging strands during cell cycle progression. While the restoration of H3K4me3 at highly transcribed genes occurs faster than at lowly expressed genes, the H3K4

[1]Institute for Cancer Genetics, Department of Pediatrics and Department of Genetics and Development, Columbia University Irving Medical Center, New York, NY 10032, USA. [2]The Hormel Institute, University of Minnesota, Austin, MN 55912, USA.
*Corresponding author. Email: zz2401@cumc.columbia.edu
†These authors contributed equally to this work.
‡Present address: Neochromosome Inc., Long Island City, NY 11101, USA.

methyltransferase COMPASS complex (*24*) is essential for the restoration, irrespective of gene transcription status. Last, we found that the plant homeodomain (PHD) finger of Spp1 (a subunit of the COMPASS complex), which binds to H3K4me3, also plays an important role in the restoration of this histone mark, especially at lowly transcribed regions, following DNA replication.

RESULTS

Parental histone asymmetry between nascent strands decreases after early S phase in *mcm2-3A* cells

We have previously shown that mutations at the HBM of Mcm2 (Mcm2-3A), a member of the CMG replicative helicase, result in an asymmetrical histone distribution of both parental and newly synthesized histones between leading and lagging strands of DNA replication forks (*21*, *22*) due to the defect in the transfer of parental histone H3-H4 to lagging strands. However, it is not known whether

this asymmetric distribution of parental and new H3-H4 at replication forks is transmitted into daughter cells. Therefore, we analyzed DNA synthesis using bromodeoxyuridine (BrdU)–immunoprecipitation (IP)–single-stranded DNA sequencing (ssSeq) and the distributions of parental (H3K4me3) and newly synthesized (H3K56ac) histone H3 at leading and lagging strands over time using eSPAN (*18*). Briefly, we synchronized wild-type (WT) and *mcm2-3A* cells at G_1 phase using α factor and then released these cells into S phase in the presence of the nucleotide analog BrdU to label nascent chromatin (Fig. 1A). Thirty minutes after release, we added thymidine to each culture to block further BrdU incorporation, and we harvested cells for H3K4me3 and H3K56ac eSPAN at 30, 60, and 90 min after the release into S phase, which correspond to early S phase, late S phase, and G_2 phase according to flow cytometry analysis of DNA content (fig. S1A). In this way, we were able to analyze the distribution of both H3K4me3 and H3K56ac in the same chromatin regions marked by BrdU over time. We observed that H3K4me3 levels in *mcm2-3A*
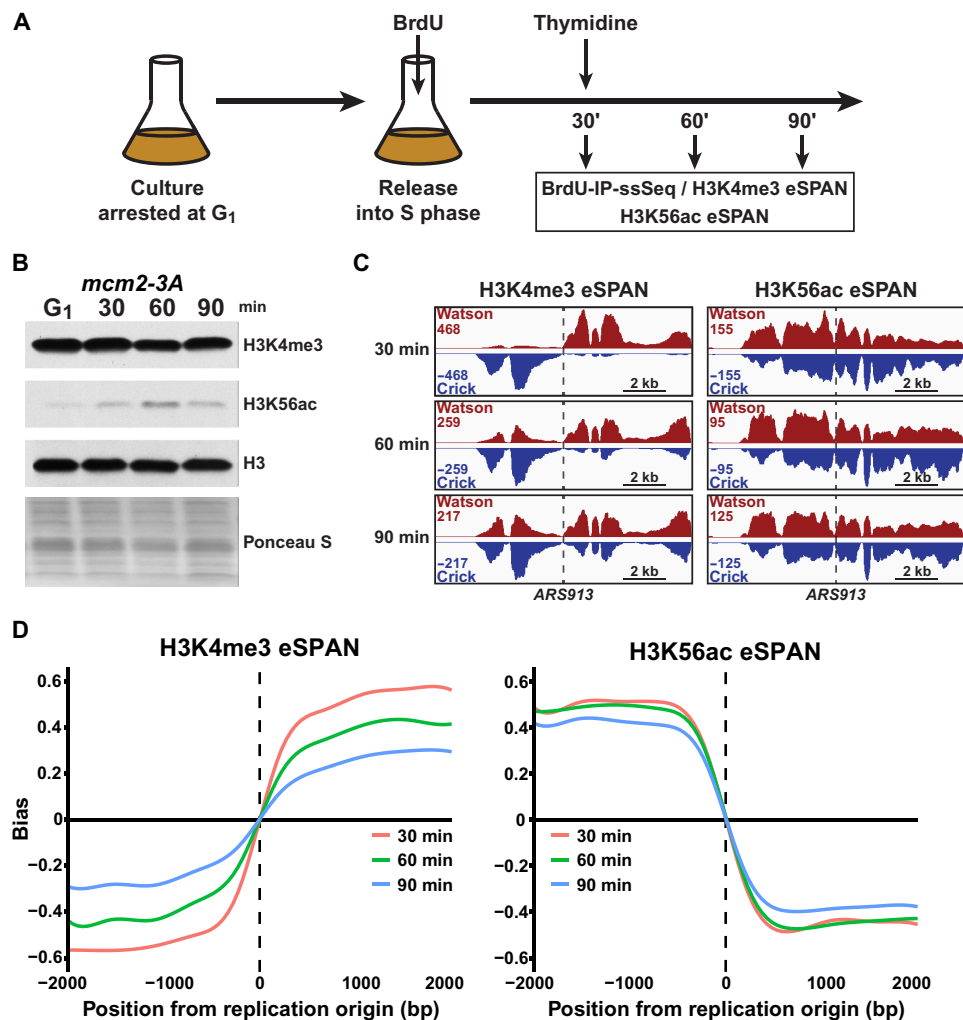
Fig. 1. The enrichment of H3K4me3 at leading strands in *mcm2-3A* is reduced during the cell cycle progression. (**A**) Outline of experimental procedures to monitor the distribution of H3K4me3 and H3K56ac at replicating chromatin during cell cycle progression. (**B**) Immunoblot analysis of the indicated proteins at G_1 and at the indicated time points after release from G_1 in *mcm2-3A* mutant cells. (**C**) Snapshots of H3K4me3 and H3K56ac eSPAN signals at Watson and Crick strands around early-firing origin *ARS913* in *mcm2-3A* cells. *Y* axis indicates reads per million reads. (**D**) Average bias of H3K4me3 (left) and H3K56ac eSPAN (right) within 4 kb of 134 early-firing replication origins at the indicated time points after release from G_1 phase in *mcm2-3A* mutant cells. One representative experiment is shown with correlation of two independent repeats shown in fig. S1B.

cells showed a mild increase at later time points, likely because of increase in histone levels during S phase, while H3K56ac signals peaked at 60 min (Fig. 1B), consistent with the idea that H3K56ac is a mark on newly synthesized H3, peaking during S phase and being removed during G_2 phase (*25, 26*). As expected, H3K4me3 eSPAN signals, which measure the relative amount of H3K4me3 between leading and lagging strands, at early-firing replication origins in *mcm2-3A* mutant cells displayed a clear leading strand bias at early S phase (30 min) (Fig. 1, C and D, and fig. S1B). However, at later time points, the bias of H3K4me3 eSPAN signals in *mcm2-3A* decreased considerably, indicating a reduction of the biased distribution of H3K4me3 between leading and lagging strands (Fig. 1, C and D, 60 and 90 min). On the other hand, H3K56ac eSPAN peaks showed a bias toward lagging strands, and this lagging strand bias was also reduced, but to lesser extent than the reduction of leading strand bias of H3K4me3 eSPAN peaks during the time course (Fig. 1, C and D, and fig. S1C). In WT cells, both H3K4me3 and H3K56ac histone marks stayed evenly distributed between the two nascent strands as the cell cycle progresses (fig. S1D). These results indicate that in *mcm2-3A*, after the initial asymmetric segregation of parental H3-H4 at replication forks due to defects in transferring parental H3-H4 to lagging strands, the differences in H3K4me3 between leading and lagging strands decrease as chromatin matures. This suggests that some mechanism(s) is acting on this histone mark to achieve a more symmetrical occupancy between nascent leading and lagging strands before cell division.

Both transcription-dependent and transcription-independent mechanisms facilitate the restoration of H3K4me3 symmetry

The H3K4me3 modification is enriched at the 5′ end of eukaryotic genes, with high levels of H3K4me3 at the promoters of actively transcribed genes (*24*). Therefore, we wondered whether gene transcription could be influencing H3K4me3 distribution between leading and lagging strands during cell cycle progression. To test this idea, we performed elongating RNA Pol II [RNA Pol II phosphorylated at its C-terminal repeat domain (CTD) Ser5] chromatin IP sequencing (ChIP-seq) following the same time course, which allows us to capture the transcriptional state of each gene at a given time point. Moreover, we focused on our H3K4me3 eSPAN analysis at the gene level (Fig. 2A). Briefly, we first defined genomic regions that had already been replicated in the early S phase time point (30 min) based on the density of BrdU-IP-ssSeq. We then selected all genes inside these replicated regions except those whose expression is regulated during cell cycle progression (640 early-replicated genes in table S3; see Materials and Methods), separated sequencing reads mapping at leading and lagging strands, and calculated H3K4me3 signals over the gene body of each early-replicated gene at each strand. At early S phase, H3K4me3 eSPAN signals were clearly enriched downstream of the transcription start site (TSS) on the leading strand compared to the same regions of the lagging strand, consistent with the strong leading strand bias of this mark in *mcm2-3A* cells (Fig. 2B). Notably, 1 hour later, the H3K4me3 eSPAN signals at both leading and lagging strands displayed a very similar profile (Fig. 2B, 90 min). This implies that after the initial defects in the transfer of H3K4me3 on lagging strands in *mcm2-3A* cells, the relative levels of H3K4me3 between both leading and lagging strands become similar.

Inspection of several early-firing replication origins suggested that gene transcription played a critical role in the restoration of H3K4me3 symmetric distribution. For instance, at the *ARS1211* locus,

we observed that, at 30 min after release, H3K4me3 eSPAN signals at replicated genes had a clear leading bias pattern with higher Crick signals on the left side of the origin and higher Watson signals on its right side (Fig. 2C). At later time points, H3K4me3 at genes with higher elongating RNA Pol II signals (*TRX1* and *PDC1*) became more symmetrical (less differences between Watson and Crick sequence reads), whereas H3K4me3 at genes with low elongating RNA Pol II signals (*AFB1* and *YLR042C*) retained a clear bias toward leading strand, suggesting that gene transcription helps restore a more symmetric distribution of H3K4me3 at the right but not the left fork. We extended the analysis to a genome-wide scale by classifying all early-replicated genes into four quartiles, with Q4 representing the top 25% highly transcribed genes and Q1 the lowest 25% transcribed genes, based on the levels of RNA Pol II CTD Ser5p ChIP-seq (Fig. 2A and fig. S2A). As expected, H3K4me3 was enriched at the 5′ end of genes compared to the gene bodies, irrespective of gene expression levels, with highly expressed genes (Q4) containing more H3K4me3 than lowly expressed ones (Q1) (fig. S2B). Genome-wide, H3K4me3 eSPAN at both Q4 and Q1 genes displayed a strong leading bias at 30 min (Fig. 2D). However, at later time points, H3K4me3 eSPAN at highly active genes showed considerably smaller bias than that at less active genes. This becomes more apparent when we analyze the bias change over time. While the H3K4me3 eSPAN bias at Q1 genes decreased mildly between 30 min and late S phase (60 min) or between 30 min and G_2 phase (90 min), the H3K4me3 eSPAN bias at Q4 genes decreased much more pronouncedly (fig. S2C). Moreover, H3K4me3 eSPAN bias change over time showed a negative correlation with elongating RNA Pol II signals on each gene (Fig. 2E). In WT cells, the H3K4me3 strand bias at early S phase was practically nonexistent (fig. S1D) regardless of gene expression (fig. S2D). These results suggest that transcription is a driving force to restore a more symmetric distribution of H3K4me3 between leading and lagging strands after the passing of the replication fork in *mcm2-3A* cells. Furthermore, as transcription was barely detectable at lowly expressed genes (fig. S2A), a transcription-independent mechanism may also exist to promote the restoration of H3K4me3 at lowly transcribed regions.

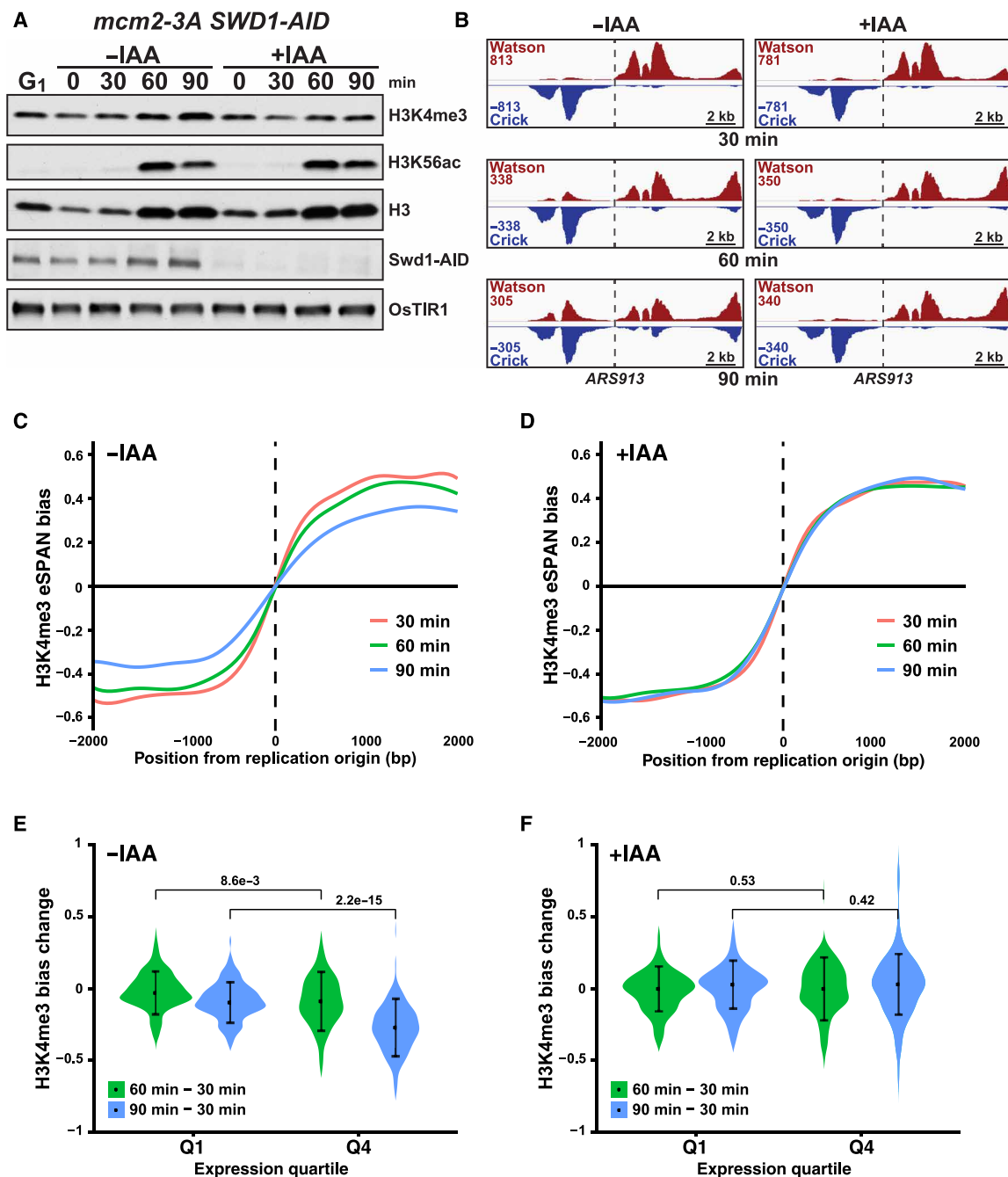**The COMPASS complex restores H3K4me3 at lagging strands in mcm2-3A cells**

As stated above, eSPAN measures the relative abundance of a histone mark between the leading and lagging DNA strands and cannot be used to estimate the abundance of H3K4me3 at either leading or lagging strands between different time points. Thus, the decrease of H3K4me3 leading bias we observed in *mcm2-3A* cells over time could be due to either a gain of H3K4me3 at lagging strands or a loss of H3K4me3 at leading strands. To differentiate these two possibilities, we decided to analyze the H3K4me3 distribution at replicating DNA strands using eSPAN in *mcm2-3A* cells where the H3K4 methyltransferase is inactivated during S phase. Specifically, we generated an *mcm2-3A* strain in which Swd1, a subunit of the COMPASS complex that is essential for the methylation of H3K4 (*24*), is tagged with the auxin-inducible degron (Swd1-AID). This allowed us to deplete Swd1 with the addition of indole-3-acetic acid (IAA), a plant hormone that induces the degradation of AID-tagged proteins. As shown in fig. S3A, after prolonged addition of IAA, Swd1-AID was degraded and H3K4me3 was markedly reduced, consistent with the results that Swd1 is essential for H3K4me3. To monitor the effect of Swd1 depletion during the progression of the
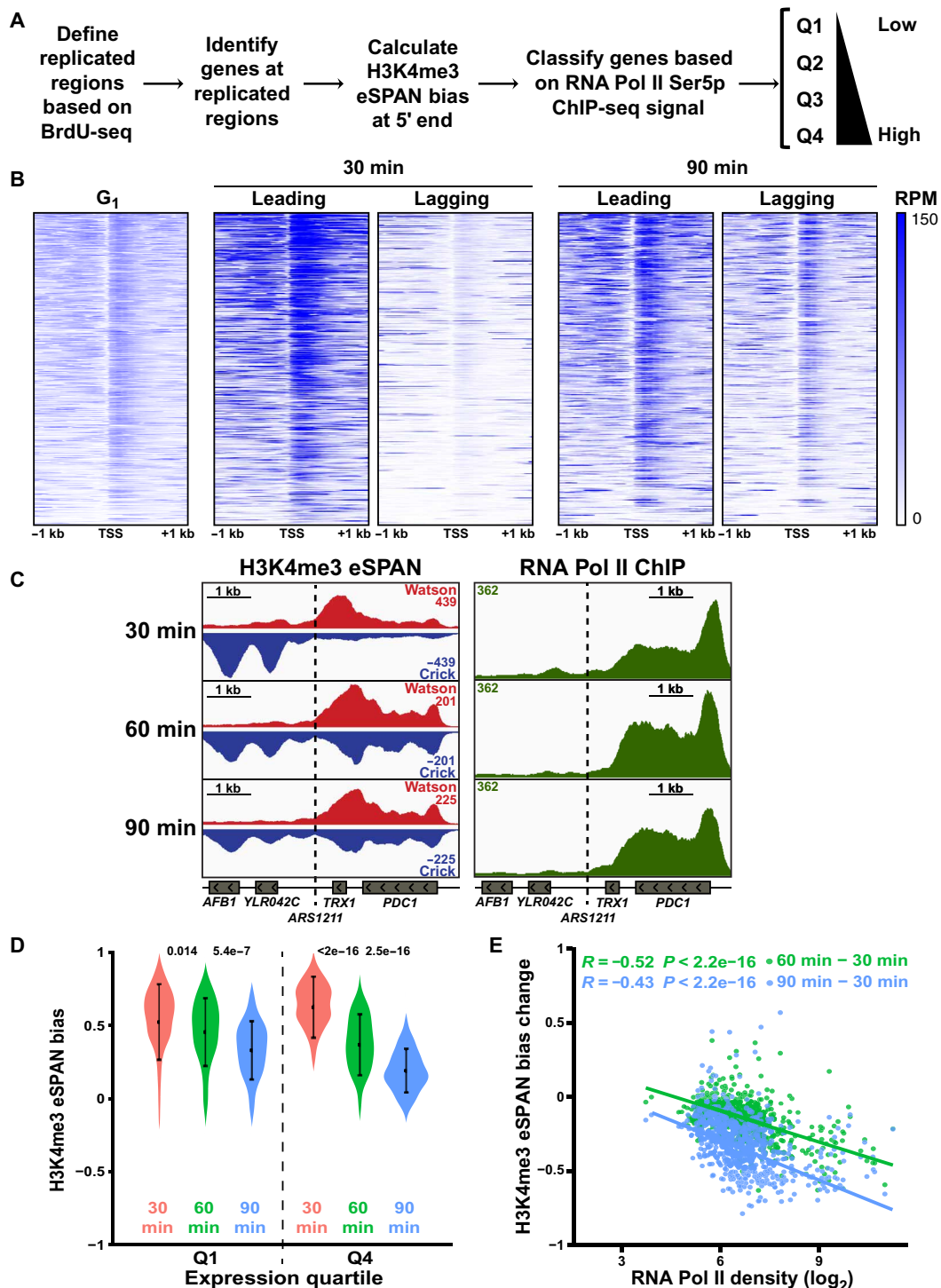
Fig. 2. Highly active genes rapidly restore H3K4me3 symmetry between leading and lagging strands. (**A**) Outline of the procedures to analyze H3K4me3 eSPAN bias in early-replicated genes that are separated into four quartiles based on the levels of RNA Pol II Ser5p. (**B**) H3K4me3 ChIP (G_1) or eSPAN (30 and 90 min) density at 2 kb around the TSS of 640 early-replicated genes. For H3K4me3 eSPAN samples, reads mapping to leading or lagging strands are plotted separately. Genes were ranked top to bottom based on H3K4me3 density at 30 min. RPM, reads per million reads. (**C**) Snapshots of H3K4me3 eSPAN sequencing reads at Watson and Crick strands (left) and RPB1 CTD Ser5p ChIP-seq (right) read density around early-firing origin *ARS1211* in *mcm2-3A* cells. *Y* axis indicates reads per million reads. (**D**) Median H3K4me3 eSPAN bias in 640 early-replicated genes classified by ongoing transcription levels, with Q1 and Q4 representing bottom 25% and top 25% genes with RPB1 CTD Ser5p ChIP-seq signal, respectively, at the indicated time points in *mcm2-3A* cells. Leading strand bias: represented by positive value; lagging strand bias: negative value; 0: no bias. *P* values from Student's *t* test are indicated. The average of two biological replicates is presented. (**E**) Relationship between elongating RNA Pol II ChIP-seq signals at 30 min and H3K4me3 eSPAN bias change for all 640 early-replicated genes in *mcm2-3A* cells from 30 to 60 min and from 30 to 90 min following the release from G_1 phase. The average of two biological replicates is presented. Pearson correlation coefficient was used to calculate the *P* value.

cell cycle, we split yeast cultures near the end of the G_1 arrest into two and added IAA to only one culture to trigger the degradation of Swd1 for 30 min (fig. S3B). We then released these G_1 phase cells into free medium either with IAA or without IAA based on the original G_1 cultures and collected cells at the indicated time points

for H3K4me3 eSPAN (fig. S3B). We observed that at the moment of release (0 min) and during all the time points of the experiment, Swd1-AID was depleted in the presence of IAA (Fig. 3A). Moreover, the slight increase in H3K4me3 over time in the culture without IAA was not detectable in cultures in the presence of IAA (compared −IAA

Fig. 3. The COMPASS complex is essential for restoring H3K4me3 at lagging strands in *mcm2-3A* cells. (**A**) Immunoblot analysis of the indicated proteins at G_1 and at the indicated time points after release into S phase in *mcm2-3A SWD1-AID* mutant cells. −IAA, culture supplemented with ethanol; +IAA, culture supplemented with IAA. (**B**) Snapshots of H3K4me3 eSPAN signals around early-firing origin *ARS913* in *mcm2-3A SWD1-AID* cells with (right) and without (left) IAA. *Y* axis indicates reads per million reads. (**C** and **D**) Average bias of H3K4me3 eSPAN within 4 kb of 134 early-firing replication origins at the indicated time points after release from G_1 into S phase in *mcm2-3A SWD1-AID* mutant cells without IAA (C) or with IAA (D). One representative experiment is shown. (**E** and **F**) Median H3K4me3 eSPAN bias change between the indicated time points at 640 early-replicated genes classified by RPB1 CTD Ser5p ChIP-seq signal (Q1, bottom 25%; Q4, top 25%) in *mcm2-3A SWD1-AID* cells without IAA (E) or with IAA (F). *P* values from Student's *t* test are indicated. The average of two biological replicates is represented.

90 min with +IAA 90 min, Fig. 3A). Under these experimental conditions, we observed that the leading bias of H3K4me3 eSPAN signals at early replication origins was reduced over time in cells without IAA (Fig. 3, B, left, and C, and fig. S3C), similar to what we have previously shown (Fig. 1). On the other hand, in the presence of IAA, there was no apparent change in the distribution of H3K4me3 between leading and lagging strands over time (Fig. 3, B, right, and D, and fig. S3D). These results indicate that when Swd1 is depleted in *mcm2-3A* cells, the asymmetric distribution of H3K4me3 at leading and lagging strands remains even when cells reach G_2 phase of the cell cycle. Furthermore, we also observed that in the absence of IAA, the decrease of leading bias of H3K4me3 eSPAN signals at highly expressed genes was more marked than that at lowly expressed genes (Fig. 3E). However, in the presence of IAA, the H3K4me3 eSPAN bias remained unaltered regardless of the transcriptional state of each gene (Fig. 3F). Overall, these results demonstrate that the COMPASS complex is essential to restore H3K4me3 to lagging strands in *mcm2-3A* cells after the initial enrichment of this mark at leading strands following the passage of DNA replication forks, irrespective of transcription.

The COMPASS complex restores H3K4me3 at leading strands in *dpb3Δ* cells

We have shown previously that because of defects in the transfer of parental H3-H4 to leading strands in cells lacking Dpb3, a subunit of Pol ε, H3K4me3 eSPAN signals in *dpb3Δ* cells show a strong lagging strand bias (*18*). We therefore determined whether the asymmetric distribution of H3K4me3 in *dpb3Δ* cells at early S phase is also reduced during cell cycle progression and, if it is, whether the reduction is mediated by a functional COMPASS complex. To this end, we generated the *dpb3ΔSWD1-AID* strain and followed the same procedures outlined in fig. S3 to degrade SWD1-AID with the addition of IAA before release into S phase. As the most marked changes of H3K4me3 eSPAN bias in *mcm2-3A* cells occurred between 30 and 90 min (Fig. 3), we analyzed the distribution of H3K4me3 at replication forks in *dpb3Δ* cells in the presence and absence of IAA at these two time points. As shown in Fig. 4A, Swd1 was depleted at G_1 upon addition of IAA, and depletion of Swd1 had minor effects on total levels of H3K4me3 in cells during this short time course. Moreover, consistent with published results (*18*), H3K4me3 eSPAN signals at 30 min exhibited a strong lagging strand bias, irrespective of the status of Swd1 (Fig. 4, B to F). In the absence of IAA, the leading strand bias of H3K4me3 eSPAN decreased markedly at 90 min compared to 30 min (Fig. 4, B, left, and C). In contrast, in the presence of IAA, the leading strand bias of H3K4me3 eSPAN signals at 90 min showed only a slight reduction compared to 30 min (Fig. 4, B, right, and D). One potential reason for the slight variation in effects of Swd1 depletion on H3K4me3 eSPAN bias observed in *dpb3Δ* compared to those in *mcm2-3A* mutant cells (unaltered H3K4me3 eSPAN bias upon depletion of Swd1 in Fig. 3D) is that the depletion of Swd1 was slightly different between these two experimental settings. We also analyzed the changes in H3K4me3 eSPAN bias in *dpb3Δ* cells at lowly expressed genes (Q1) and highly expressed genes (Q4). We found that the H3K4me3 eSPAN bias was reduced much more at Q4 genes than Q1 genes in the absence of IAA (Fig. 4G). In the presence of IAA, the reduction of H3K4me3 lagging strand bias at Q4 genes from 90 to 30 min was similar to that of Q1 (Fig. 4H), consistent with the idea that depletion of Swd1 inhibits the restoration of H3K4me3 in *dpb3Δ* cells following DNA

replication. Together, these results indicate that the asymmetric distribution of H3K4me3 at early S phase in *dpb3Δ* cells is also reduced markedly before cells enter mitosis, and the COMPASS complex also plays a critical role in this process.

### Spp1 is important for H3K4me3 restoration after DNA replication

We have shown that in *mcm2-3A* cells the initial defect in H3K4me3 levels at lagging strands is reverted by the COMPASS complex, which likely acts on the nucleosomes containing newly synthesized H3 without this histone mark. Because genes showing low or no elongating RNA Pol II also showed recovery of H3K4me3 at lagging strands (Fig. 2D, Q1 genes), we wondered whether, in addition to gene expression, some other mechanism promotes H3K4 methylation restoration after the passing of the replication fork. A common mode of histone PTM reestablishment such as H3K9 methylation and H3K27 methylation is by a read-write mechanism whereby their corresponding enzymes can specifically recognize their cognate modifications (read), which in turn direct the enzymes to modify neighboring nucleosomes without this mark (write) (*12–14*). It has been recently shown that Spp1, another member of the COMPASS complex, contains a PHD finger that specifically binds to H3K4me3 (*27*). Moreover, the recognition of H3K4me3 by Spp1 helps to recruit the Rec114-Mei4-Mer2 complex to double-strand breaks during meiosis (*28–30*). However, to what extent the recognition of H3K4me3 by Spp1 helps the restoration of this mark following DNA replication was not known. Therefore, we performed multiple sets of experiments described below to test whether Spp1 could help recruit the COMPASS complex for the restoration of H3K4me3, especially at regions with low gene transcription. First, we investigated the effects of acute Spp1 depletion on the distribution of this mark between leading and lagging DNA strands in *mcm2-3A* cells during cell cycle progression. Addition of IAA for 8 hours led to a notable reduction of Spp1-AID and a reduction of H3K4me3, but to a lesser extent than Swd1-AID depletion (Fig. 5A), consistent with a previously published report that Spp1 is not essential for H3K4 methylation (*31*). We then analyzed the distribution of H3K4me3 in *mcm2-3A* cells with or without Spp1 depletion during G_1 phase of the cell cycle following the similar procedures as in Fig. 3 and fig. S3B (Fig. 5B). In cells without IAA, we observed a marked decrease in leading strand bias of H3K4me3 eSPAN during cell cycle progression (Fig. 5, C and E). In contrast, this reduction was much less pronounced with the addition of IAA (Fig. 5, D and F). The small reduction of H3K4me3 leading strand bias after Spp1 depletion likely reflects the fact that cells lacking Spp1 contain residual H3K4me3 activity (Fig. 5A). Last, under these conditions, without IAA, we observed an obvious strong decrease in H3K4me3 eSPAN bias at highly expressed genes (Q4) compared to lowly expressed genes (Q1), while in the presence of IAA both highly and lowly expressed genes showed a similar bias change over time (Fig. 5, G and H). These results indicate that Spp1 is important, but not essential, for the restoration of H3K4me3 during cell cycle progression.

The PHD finger of Spp1 is important for H3K4me3 restoration after DNA replication

It has been shown that mutations at PHD finger of Spp1 resulted in reduced H3K4me3 levels (*31*). Therefore, we generated a strain with the W45A mutation at *SPP1*, which abrogates the ability of the PHD domain of Spp1 to bind H3K4me3 (*27*), and analyzed how
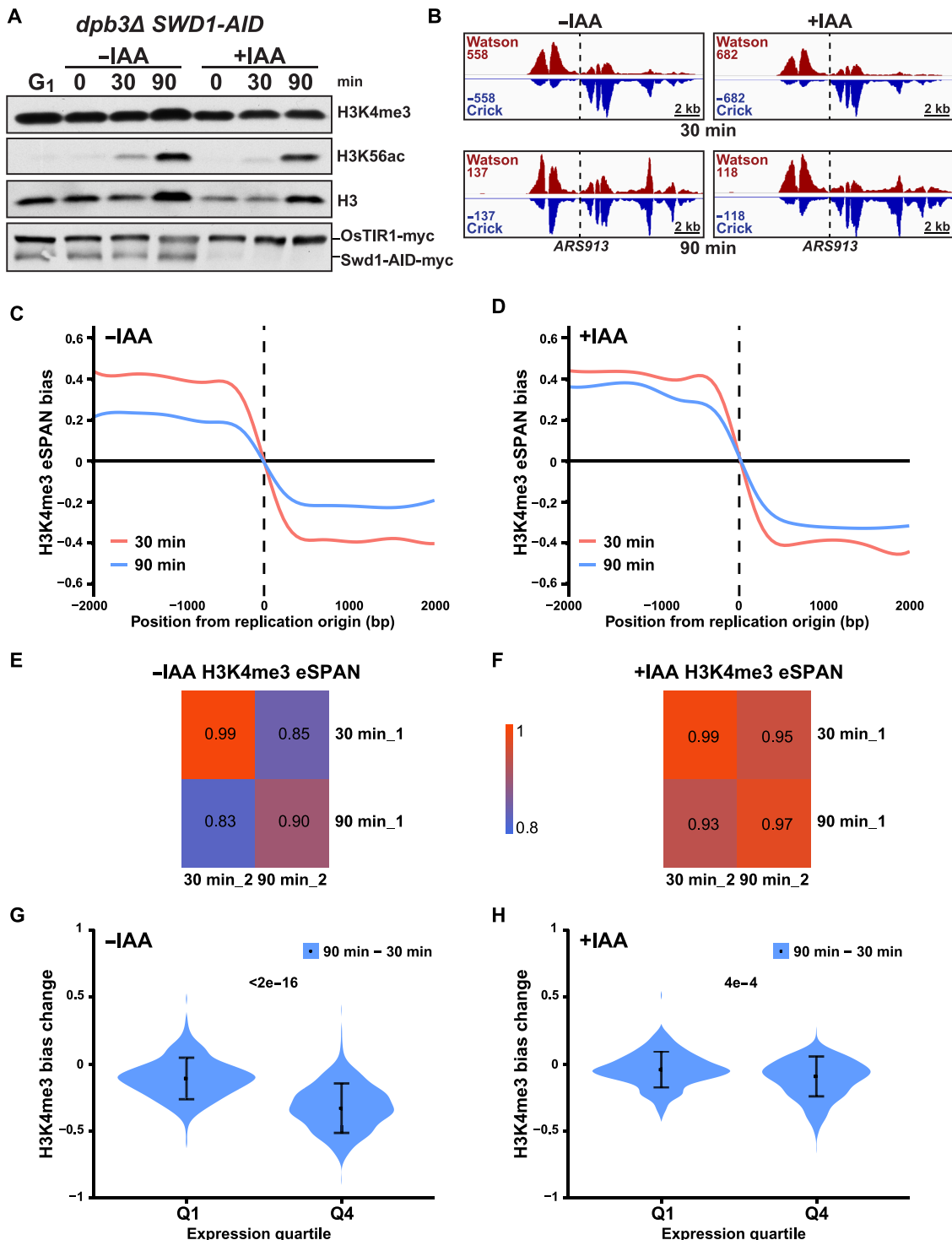
Fig. 4. The COMPASS complex is essential for restoring H3K4me3 at leading strands in *dpb3Δ* cells. (**A**) Immunoblot analysis of the indicated proteins at G_1 and at the indicated time points after release into S phase in *dpb3Δ SWD1-AID* mutant cells. −IAA, culture supplemented with ethanol; +IAA, culture supplemented with IAA. (**B**) Snapshots of H3K4me3 eSPAN showing Watson and Crick sequence read densities around early-firing origin *ARS913* in *dpb3ΔSWD1-AID* cells with (right) and without (left) IAA. *Y* axis indicates reads per million reads. (**C** and **D**) Average bias of H3K4me3 eSPAN within 4 kb of 134 early-firing replication origins at the indicated time points after release from G_1 into S phase in *dpb3ΔSWD1-AID* mutant cells without IAA (C) or with IAA (D), with one presentative experiment shown. (**E** and **F**) Correlation matrix of two biological replicates of H3K4me3 eSPAN signals within 4 kb of 134 early-firing replication origins at the indicated time points after release into S phase in *dpb3Δ SWD1-AID* cells without IAA (E) or with IAA (F). Values indicate Pearson's correlation. (**G** and **H**) Median H3K4me3 eSPAN bias change between the indicated time points at 640 early-replicated genes classified by RPB1 CTD Ser5p ChIP-seq signal (Q1, bottom 25%; Q4, top 25%) in *dpb3ΔSWD1-AID* cells without IAA (G) or with IAA (H). *P* values from Student's *t* test are indicated. The average of two biological replicates is represented.
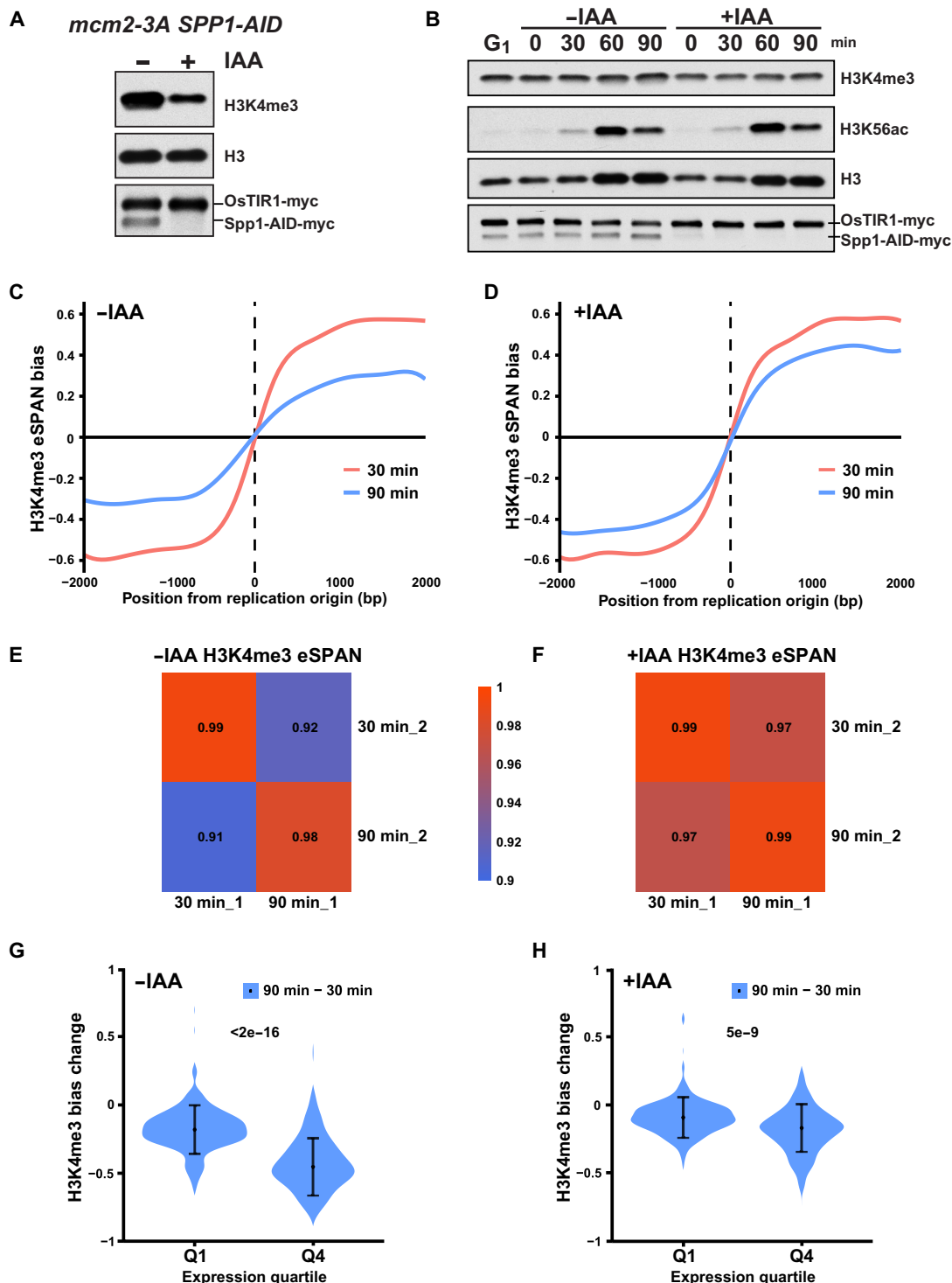
Fig. 5. Role of Spp1 subunit of the COMPASS complex in the restoration of H3K4me3 following DNA replication. (**A**) Immunoblot analysis of the indicated proteins in *mcm2-3A SPP1-AID* mutant cells. Exponentially growing cells were divided into two and treated with ethanol (−IAA) or with IAA for 8 hours. (**B**) Immunoblot analysis of the indicated proteins in *mcm2-3A SPP1-AID* mutant cells at G_1 and at the indicated time points after release into S phase from the G_1 arrest in the absence (−IAA) or presence (+IAA) of IAA. (**C** and **D**) Average H3K4me3 eSPAN strand bias within 4 kb of 134 early-firing replication origins in *mcm2-3A SPP1-AID* cells at the indicated time points after release into S phase without IAA (C) or with IAA (D). One representative experiment is shown. (**E** and **F**) Correlation matrix of two biological replicates of H3K4me3 eSPAN signals within 4 kb of 134 early-firing replication origins at the indicated time points after release into S phase in *mcm2-3A SPP1-AID* cells without IAA (E) or with IAA (F). Values indicate Pearson's correlation. (**G** and **H**) Median H3K4me3 eSPAN bias change between 90 and 30 min at 640 early-replicated genes classified by CTD Ser5p ChIP-seq signals (Q1, bottom 25% in RPB1; Q4, top 25%) in *mcm2-3A SPP1-AID* cells without IAA (G) or with IAA (H). P values from Student's t test are indicated. The average of two biological replicates is represented.

this mutation affected H3K4me3 using the following assays. First, Western blot analysis showed that this mutation led to a mild but significant reduction of overall levels of H3K4me3 compared to WT (Fig. 6A) (*31*). Next, we compared the H3K4me3 levels on chromatin between WT and *spp1-W45A* mutant at G_1 phase to eliminate the effects of cell cycle and normalized H3K4me3 levels using spike-in H3K4me3 ChIP-seq. We observed that H3K4me3 around the TSS at G_1 in *spp1-W45A* cells was markedly reduced compared to WT cells (Fig. 6B), supporting the idea that the PHD finger of Spp1 is needed for H3K4me3 methylation. Third, to determine whether the PHD finger is needed for H3K4me3 restoration during cell cycle progression, we arrested WT and *spp1-W45A* cells at G_1, released these cells into the cell cycle, and analyzed H3K4me3 levels every 30 min following release using ChIP-seq (fig. S4A). To accurately compare H3K4me3 ChIP-seq signals at different time points between WT and *spp1-W45A,* we added *Schizosaccharomyces pombe* cells into each sample as spike-in. Moreover, as the levels of H3K4me3 at G_1 in WT were different from those in *spp1-W45A* cells (Fig. 6B), we analyzed H3K4me3 density at early-replicated genes as a ratio between H3K4me3 ChIP-seq signals at each time point and those at G_1 (fig. S4B). After release into S phase, both WT and *spp1-W45A* showed a similar pattern of H3K4me3 signal at the TSS of early-replicated genes. H3K4me3 density decreases during S phase, reaching its lowest point 60 min after release (end of S phase), corresponding to around half of the initial G_1 density, which reflects the dilution of this mark due to an increase in DNA content from G_1 to S phase during DNA replication (see Materials and Methods). Afterward, in WT cells, H3K4me3 levels started to increase, reaching their maximum density at the G_2-M phase (120 min), without increasing further in the next G_1 phase (150 min). This maturation dynamics are consistent with H3K4me3 restoration in human cells in that restoration of H3K4me3 also occurs at G_1 before cells enter the next S phase (*32*). In contrast, *spp1-W45A* mutant cells show a slower recovery of H3K4me3 than WT cells, reaching the maximum levels at the next G_1 phase (150 min). These results indicate that the PHD finger of Spp1 is important for the restoration of H3K4me3 levels following DNA replication.

It is possible that the reduced recovery in H3K4me3 in *spp1-W45A* mutant cells detected above is due to the initially reduced levels of H3K4me3 at G_1 phase compared to WT cells (Fig. 6B). To rule out this possibility and to monitor the impact of *spp1-W45A* mutation on the restoration of H3K4me3 during cell cycle more accurately, we decided to induce the expression of either Spp1 or Spp1-W45A at the same time as we depleted the endogenous Spp1-AID protein before release from G_1 arrest. In this way, initial H3K4me3 levels would be similar in cells expressing Spp or Spp1-W45A proteins during cell cycle progression. Briefly, we inserted a hemagglutinin (HA)–tagged copy of WT or mutant Spp1-W45A under a galactose-inducible promoter (*GAL-SPP1-HA* or *GAL-spp1-W45A-HA*) into the *SPP1-AID* strain described above. To study H3K4me3 recovery during cell cycle progression, we arrested cells at G_1 with α factor and, during the second half of the arrest, we added IAA to deplete endogenous Spp1-AID and galactose to induce the expression of Spp1-HA or Spp1-W45A-HA (Fig. 6C). Cells were then released into fresh medium also containing IAA and galactose and collected periodically for H3K4me3 ChIP. Western blot analysis indicated that pre-G_1 cells only expressed Spp1-AID (pre-G_1), whereas, after adding IAA and galactose, Spp1-AID was depleted, and Spp1-HA and Spp1-W45A-HA were expressed at similar levels (Fig. 6D). Cell

cycle analysis showed that although almost all cells were arrested at G_1, only half the cells are released into the cell cycle under the experimental conditions with galactose as the main carbon source for yeast growth as compared to glucose, the preferred carbon source for yeast (fig. S4C). Likewise, under these conditions, it took longer (45 min compared to 30 min) for cells to start S phase from G_1 arrest than when growing in the presence of glucose (fig. S4C). H3K4me3 ChIP-seq density at the TSS in *GAL-spp1-W45A* cells at G_1 was very similar to cells expressing *GAL-SPP1* before release into S phase (Fig. 6E). However, after release from G_1, H3K4me3 density at early-replicated genes in *spp1-W45A* cells was lower than WT, and this difference increased over time until 105 min. Furthermore, H3K4me3 levels at early-replicated genes as a ratio of the G_1 sample were reduced more markedly in Spp1-W45A mutant compared to Spp1 WT cells in all time points after 45 min (Fig. 6F). These results indicate that the W45A mutation impairs the recovery of H3K4me3 at early-replicated genes. Last, we also analyzed recovery rate of H3K4me3 at early-replicated genes with different expression levels after normalization against H3K4me3 at G_1. Shortly after release (45 min), H3K4me3 density at both lowly (Q1) and highly (Q4) expressed genes was similar between Spp1 and Spp1-W45A (Fig. 6G). However, the recovery rate of H3K4me3 at lowly and highly expressed genes at replication forks in *spp1-W45A* mutant cells was reduced compared to WT cells, with more pronounced defects at lowly expressed genes. These results support the idea that the binding of H3K4me3 by Spp1 contributes to the restoration of H3K4me3 at both highly and lowly expressed genes, with a more pronounced role for lowly expressed genes.

To provide additional evidence that Spp1 binding to H3K4me3 is important for the restoration of H3K4me3 at inactive genes, we analyzed the effects of *spp1-W45A* mutant on the restoration of H3K4me3 at genes regulated by α factor. On the basis of the density of elongating RNA Pol II and published microarray data sets (GSE8982), we identified 79 genes that are up-regulated compared to other phases of the cell cycle in the presence of α factor (fig. S5A). The expression of these genes was reduced markedly when cells enter S phase of the cell cycle (fig. S5, B and C). Please note that most of these genes are located further from early replication origins and were not included in the 640 early-replicated genes listed in table S3. We then calculated H3K4me3 density compared to G_1 at these genes in Spp1 WT and *spp1-W45A* cells during the cell cycle progression. We found that H3K4me3 levels at these genes in *spp1-W45A* mutant cells were lower than in Spp1 WT cells during cell cycle progression, suggesting that the H3K4me3 binding by Spp1 is also important for restoration of this mark at inactive genes under vegetative growth (fig. S5, D and E). Together, these results strongly support the idea that recognition of H3K4me3 by Spp1 helps restore H3K4me3 following DNA replication, particularly at inactive genes.

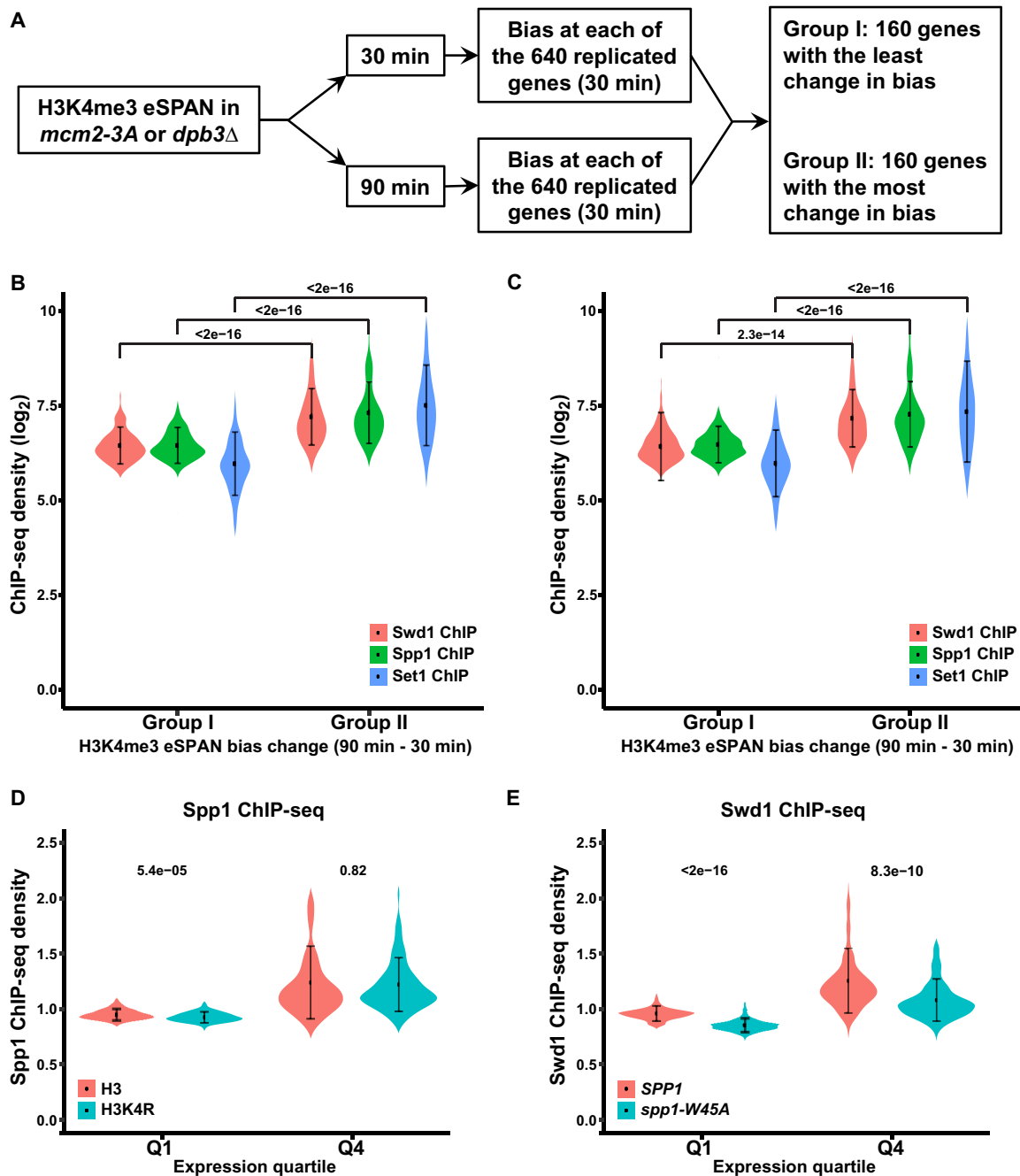## The recognition of H3K4me3 by the Spp1 PHD domain helps recruit the COMPASS complex to chromatin

To further test the idea that recognition of H3K4me3 by Spp1 facilitates the restoration of this mark following DNA replication, we analyzed whether the levels of the COMPASS complex at regions with different recovery rate in *mcm2-3A* and *dpb3Δ* mutant cells are different. Toward this end, we first calculated changes in H3K4me3 eSPAN bias at 640 early-replicated genes listed in table S3 between 90 and 30 min in *mcm2-3A* or *dpb3Δ* mutant cells and selected the top 25% genes with the least reduction in H3K4me3 eSPAN bias
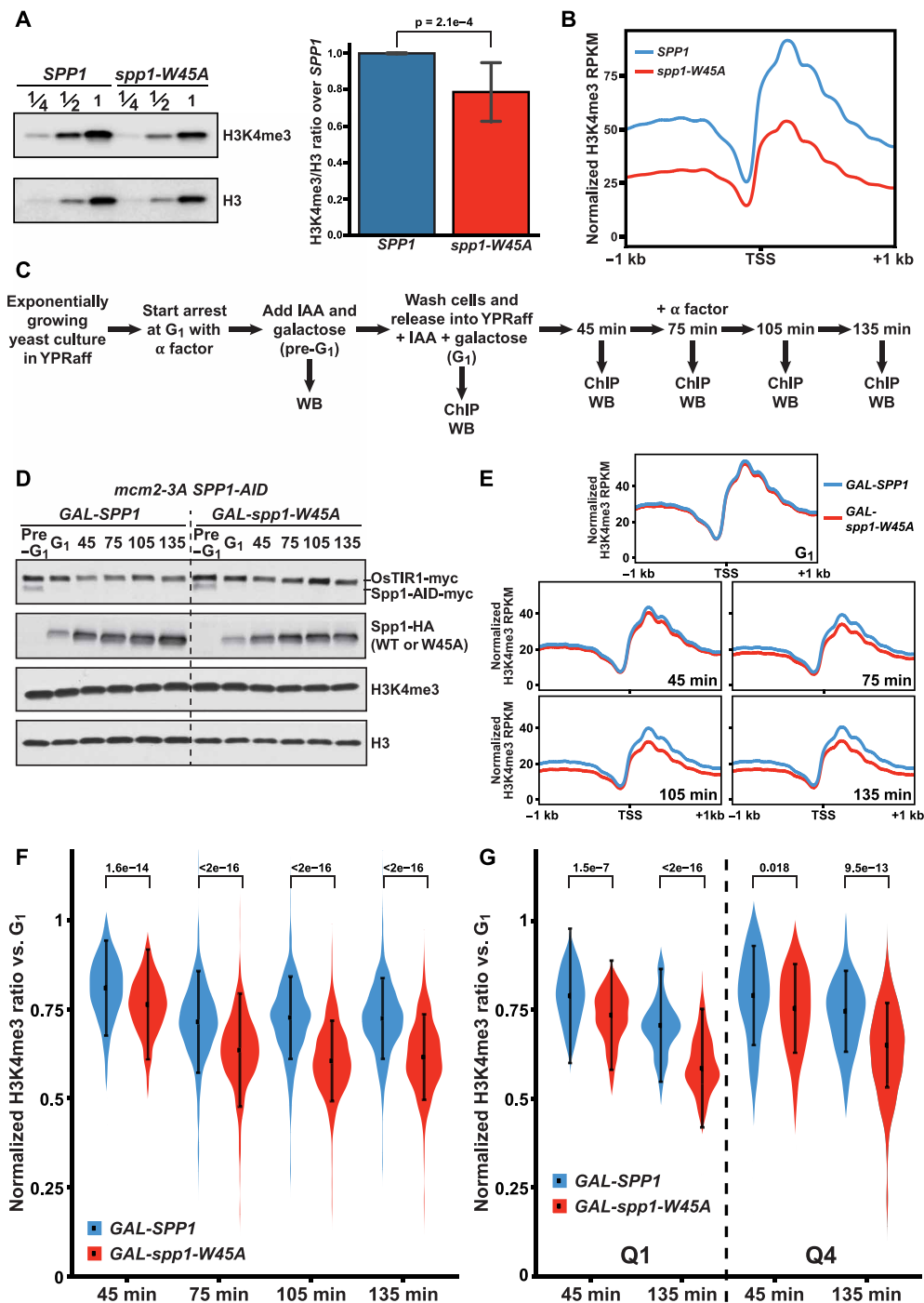
Fig. 6. Spp1 PHD finger domain is important for restoration of H3K4me3 levels during cell cycle progression. (**A**) Effects of spp1-W45A mutation on H3K4me3 levels. Left: representative immunoblot analysis of H3K4me3 and H3 at serial dilutions of the same protein extracts in *SPP1* and *spp1-W45A* cells. Right: average H3K4me3 normalized against H3 in WT and *spp1-W45A* cells. The average ratio was calculated from eight different data points corresponding to three biological replicates. Error bars represent the SD and *P* value of Wilcoxon's one-sided test. (**B**) Spike-in normalized H3K4me3 ChIP-seq signal at 2 kb around the TSS of all genes in *SPP1* and *spp1-W45A* cells synchronized at G_1. RPKM, reads per kilobase per million reads. The average of two biological replicates is represented. (**C**) Experimental outline to analyze H3K4me3 levels by Western blot and by ChIP assays during cell cycle progression after depletion of *SPP1-AID* and induced expression of *GAL-SPP1* or *GAL-spp1-W45A*. WB, Western blot. (**D**) Immunoblot analysis of the indicated proteins at the indicated time points in *GAL-SPP1* and *GAL-spp1-W45A* cells. (**E**) Spike-in normalized read density of H3K4me3 ChIP signals at 2 kb around the TSS of 640 early-replicated genes in *GAL-SPP1* and *GAL-spp1-W45A* cells at G_1 or the indicated time point after release into S phase. RPKM, reads per kilobase per million reads, with the average of two biological replicates shown. (**F** and **G**) Ratio of H3K4me3 spike-in normalized read density at the promoters (between 200 bp upstream and 500 bp downstream of TSS) of 640 early-replicated genes between each time point after release into S phase and G_1 phase in *GAL-SPP1* and *GAL-spp1-W45A* cells. Q1 and Q4: bottom and top 25% genes classified by transcription elongation as in Fig. 2A (G). *P* values from Student's *t* test are indicated. The average of two biological replicates is represented.

(group I, 160 genes) and the 25% genes with the most reduction of H3K4me3 eSPAN bias (group II, 160 genes) (Fig. 7A). We then calculated the levels of Set1, the catalytic subunit of the COMPASS complex, at these two groups of genes using published Set1 ChIP-seq dataset (33). We found that Set1 levels were higher at group II genes

compared to group I genes (Fig. 7B). Similar results were obtained when compared to group I and group II genes identified in *dpb3Δ* mutant cells (Fig. 7C). To extend this analysis, we performed Swd1 ChIP-seq using yeast cells synchronized at G_1 and Spp1 ChIP-seq using asynchronous yeast cells and compared the levels of Swd1 and

Fig. 7. Recognition of H3K4me3 by Spp1 helps recruit the COMPASS complex to chromatin for the restoration of this mark. (**A**) Outline for the classification group I and group II genes with the least and the most reduction of H3K4me3 eSPAN bias over time in either *mcm2-3A* or *dpb3Δ* cells, respectively. (**B** and **C**) Normalized read density of Swd1, Spp1, and Set1 ChIP-seq, subunits of the COMPASS complex, at identified group I and group II replicated gene set in *mcm2-3A* (B) and *dpb3Δ* (C) cells. Please note that Spp1 and Set1 ChIP-seq were performed in WT yeast cells. Swd1 ChIP-seq was performed in *mcm2-3A* cells. *P* values from Student's *t* test are indicated. The average of two biological replicates is represented. (**D**) Spp1 ChIP-seq density normalized using untagged Spp1 strain highly (Q4) and lowly expressed (Q1) of early-replicated genes in WT and H3K4R mutant cells. (**E**) Swd1 ChIP-seq density normalized using nontagged Swd1 strain at Q1 and Q4 early replicated in *SPP1* and *spp1-W45A* cells. The results from (D) and (E) represent the average of two biological replicates and *P* values from Student's *t* test.

Spp1 at these two groups of genes. We found that the Swd1 and Spp1 levels were also higher at group II genes, with the most reduction in H3K4me3 eSPAN bias, compared to group I genes with the least reduction. Together, these results support the idea that the amount of the COMPASS complex plays an important role in determining the rate of restoration of H3K4me3 levels following DNA replication.

Next, we tested whether recognition of H3K4me3 by Spp1 helps recruit Spp1 to chromatin. To do this, we performed Spp1 ChIP-seq in WT and H3K4R mutant cells and compared the levels of Spp1 at lowly expressed and highly expressed genes. The association of Spp1 with lowly expressed genes was reduced in H3K4R mutant cells compared to WT cells (Fig. 7D). In contrast, the levels of Spp1 at highly transcribed genes were similar between WT and H3K4R mutant. The inability to detect the effects of H3K4R mutation on the binding of Spp1 at highly transcribed genes is likely due to the fact that the driving force for the recruitment of the COMPASS complex to these regions is through transcription machinery, which could potentially mask smaller defects caused by the H3K4R mutation. Nonetheless, these results are consistent with the idea that Spp1 binding to H3K4me3 helps the recruitment of the COMPASS complex, including Spp1 to chromatin, and this mechanism is likely more important at chromatin regions without ongoing transcription.

Last, we tested the effects of *spp1-W45A* mutation on Swd1 chromatin binding. To do this, we performed Swd1 ChIP-seq in WT and *spp1-W45A* mutant cells using cells at G_1 phase of the cell cycle for two reasons. First, in mammalian cells, the recovery of H3K4me3 starts with S phase and continues at G_1 phase of the cell cycle (*32*, *34*). Second, by analysis of the levels of Swd1 at G_1, we can reduce potential artifacts arising from normalization from different DNA content during different phases of the cell cycle. We found that Swd1 levels at both lowly transcribed and highly transcribed genes were reduced in *spp1-W45A* compared to WT cells (Fig. 7E). Together, these results support the idea that recognition of H3K4me3 by Spp1 facilitates the recruitment of the COMPASS complex to chromatin, with a more pronounced role at lowly transcribed regions, for the restoration of H3K4me3 to newly synthesized H3 following DNA replication.

DISCUSSION

In recent years, several members of the replisome have been found to be involved in the transfer of parental H3-H4 to replicating DNA strands. Mutations at the HBM of Mcm2 or Pol1 or loss of Dpb3/Dpb4 results in a marked asymmetry in parental H3-H4 segregation between leading and lagging strands immediately following DNA synthesis (*18*, *19*, *21*, *22*). These studies focused on the segregation of parental histones on newly replicated chromatin without monitoring its maturation outside of S phase. Here, we analyzed the changes in H3K4me3 distribution between leading and lagging strands at early-replicated chromatin into late S phase and G_2 phase. We found that the enrichment of parental H3K4me3 at leading and lagging strands in *mcm2-3A* and *dpb3Δ* cells, respectively, is reduced to half from early S phase to G_2 phase, suggesting that the disparities between leading and lagging strands become considerably smaller before cell division. We suggest that the asymmetrical parental histone distribution with their specific modifications during DNA replication is not a preferred outcome for cells undergoing symmetric cell division.

We show that depletion of Swd1 in *mcm2-3A* or *dpb3Δ* mutant cells, a subunit of the COMPASS complex that is essential for

H3K4me3 enzymatic activity, largely inhibits the restoration of H3K4me3 symmetry, irrespective of transcription status. These results indicate that the primary mechanism for the restoration of H3K4me3 at replicated DNA strands to a more symmetric distribution in these mutant cells is methylation of nucleosomes without H3K4me3, not by demethylation of this mark on parental histones.

Our results indicate that at least two mechanisms contribute to the recruitment of the COMPASS complex to restore H3K4me3. First, we observed that H3K4me3 at highly transcribed genes is recovered faster than at lowly expressed genes, suggesting that gene transcription plays a role in the restoration of this mark between leading and lagging strands. It is known that the COMPASS complex is recruited to active genes by its interaction with RNA Pol II (*35*). Therefore, it is likely that the COMPASS complex is recruited to actively transcribed regions following DNA replication, contributing to the restoration of H3K4me3 at these regions (fig. S6A). Supporting this idea, we found that the levels of three components (Spp1, Set1, and Swd1) of the COMPASS complex analyzed at genes with the most reduction in H3K4me3 eSPAN asymmetry were higher than at genes with least reduction. Second, we show that recognition (read) of H3K4me3 by the PHD finger of Spp1, a subunit of the COMPASS complex, also contributes to the restoration of this mark on unmodified nucleosomes (write) during cell cycle progression (fig. S6, B to D). Supporting this idea, we found that H3K4me3 eSPAN bias at genes with practically no elongating RNA Pol II signals in *mcm2-3A or dpb3Δ* cells is also reduced over time. Furthermore, a single point mutation in Spp1 (*spp1-W45A*) that impairs H3K4me3 binding results in a delayed recovery of H3K4me3 on chromatin, especially at lowly transcribed regions, following DNA replication. We observed that the chromatin binding of Spp1 is reduced at lowly expressed genes in H3K4R mutant cells, and the levels of Swd1 at chromatin are reduced in *spp1-W45A* mutant cells. Together, these results strongly support the idea that recognition of H3K4me3 by the Spp1 PHD domain helps recruit the COMPASS complex to chromatin for the restoration of this mark on newly synthesized histones following DNA replication.

In the *mcm2-3A* mutant cells, H3K4me3 levels at lagging strand are lower than the corresponding leading strand. One would expect that the read-write mechanism by Spp1 would be less efficient at lagging strands because of potential gaps from missing H3K4me3 nucleosomes in the mutant cells. Why is then H3K4me3 at lagging strand recovered faster than that at leading strand during the cell cycle progression? We discuss the following possibilities. First, it is possible that the restoration of H3K4me3 at lagging strand in *mcm2-3A* mutant cells relies on reading of H3K4me3 on leading strand of the second fork originated from the same replication origin. Second, alternatively, Spp1 reads H3K4me3 on leading strand of the same fork at different chromatid (fig. S6, B to D). Third, we suggest that the faster recovery at lagging strands of *mcm2-3A* mutant cells is likely due to an increase in nucleosomes with H3K56ac. Consistent with this idea, we observed that H3K56ac eSPAN shows a lagging strand bias. Therefore, the local concentration of nucleosomes to be methylated by the COMPASS complex on lagging strands is higher than that at corresponding leading strand, which, in principle, can compensate for lower levels of H3K4me3 recognized by Spp1. Future studies are needed to test these and other hypotheses.

The "read and write" mechanism has been shown previously to mediate the inheritance of two silent marks (H3K9me3 and H3K27me3) from fission yeast to mammalian cells (*12*–*14*). In general,

the distribution of H3K9me3 and H3K27me3 is broad at these heterochromatin regions. In addition to the enrichment at the promoter-proximal regions of actively transcribed genes, H3K4me3 is also found, albeit at lower levels, at lowly expressed genes (fig. S2B) (*36*). Moreover, it has been shown that there exists a noncanonical form of H3K4me3 consisting of broad H3K4me3 peaks at the promoters and distal loci. These broad H3K4me3 domains can be inherited in preimplantation embryos before being erased at two-cell embryo stages (*37*, *38*). Therefore, it is possible that the read-write mechanism for H3K4me3 described here plays a large role in the restoration of this mark at these chromatin regions.

The mechanisms for the restoration of H3K4me3 described here may also contribute to epigenetic memory of active gene transcription states during reprograming. It has been shown that active gene states of donor cell nuclei are retained for 24 cell divisions when an endoderm cell nucleus is transplanted to an enucleated egg in the absence of the conditions for the induction of the active gene states. This memory of active gene transcription depends on histone H3 variant H3.3 and status of histone H3 lysine 4. Mutating H3 lysine 4 eliminates this memory, suggesting that H3 lysine 4 methylation, the dominant form of H3 modification at this position, likely plays a role in the memory of the active gene transcriptional states (*39*). Consistent with this idea, it has been shown that H3K4 methylation–mediated memory of active transcriptional states in somatic cells is a roadblock that limits transcriptional reprogramming (*40*). At organismal levels, H3K4me3 methylation complex and its associated gene expression in *Caenorhabditis elegans* are linked to transgenerational epigenetic inheritance of life span (*41*). In mouse, histone H3K4 methylation plays a role in learning and memory (*42*). We suggest that molecular mechanisms on restoration of H3K4me3 after DNA replication described here, including the read and write mechanism, may facilitate the maintenance of H3K4me3 levels and the transcriptional states in these settings.

MATERIALS AND METHODS

Yeast strains
All yeast strains used in this study are of the W303-1A genetic background (*MAT**a** leu2-3*, *112 ura3-1 his3-11*, *trp1-1*, *ade2-1 can1-100*) and listed in table S1. Mutagenesis was performed using polymerase chain reaction (PCR)–based methods (*43*) or by CRISPR-Cas9–mediated editing using the pML104 plasmid (*44*) with the primers described in table S2 for the strain ASC379. Strains ASC387 and ASC389, containing the *SPP1* or *spp1-W45A* gene under the *GAL1* promoter and followed by 3HA tags, were constructed as follows: The 3HA tags were introduced into strains CYC520 and ASC379 using PCR-based methods. The *SPP1/spp1-W45A-3HA* gene was PCR-amplified and cloned into p414GAL1 (*45*) with Eco RI/Xho I. Last, the *TRP1-GAL1-SPP1/spp1-W45A-3HA* cassette was inserted into the *trp1-1* locus of strain ASC371 following PCR-based methods.

Yeast culture conditions
Yeast cells were grown in rich medium (1% yeast extract, 2% peptone) supplemented with 2% glucose (YPD) or, for galactose induction experiments, with 2% raffinose (YPRaff). Exponentially growing cells were arrested at G_1 phase with α factor (5 μg/ml; EZBiolab) for 3 hours (YPD) or 3.5 hours (YPRaff). Degradation of AID-tagged proteins was achieved with the addition of 1 mM IAA (I2886, Sigma-Aldrich) into the medium. Induction of proteins under the *GAL1* promoter was achieved with the addition of 2% galactose into YPRaff.

Chromatin IP
For time course ChIP experiments, exponentially growing cells in YPD were arrested at G_1 with α factor as described above. For Spp1 complementation experiments, exponentially growing cells in YPRaff were arrested at G_1, induction of *GAL-SPP1* or *GAL-SPP1-W45A* was accomplished with the addition of 2% galactose, and degradation of AID-tagged proteins was performed by supplementing IAA. Arrested cells were collected by centrifugation, washed twice with cold H_2O, and released in fresh medium at 25°C (YPD) or 30°C (YPRaff + 2% galactose) in the presence of BrdU (400 μg/ml; B5002, Sigma-Aldrich) when indicated. To block further BrdU incorporation, thymidine (3.15 mg/ml; T1895, Sigma-Aldrich) was added 30 min after release. At the indicated time points, 50 ml of culture was cross-linked with 1% paraformaldehyde for 20 min at room temperature followed by quenching with 125 mM glycine for 5 min at room temperature. For experiments using spike-in normalization, cross-linked *S. pombe* cells corresponding to 10% of OD (optical density) of each sample were added. Cells were collected by centrifugation, resuspended in ChIP lysis buffer [50 mM Hepes/KOH (pH 7.5), 140 mM NaCl, 1 mM EDTA, 1% Triton X-100, and 0.1% Na-deoxycholate containing 1× SIGMAFAST Protease Inhibitor cocktail (S8830, Sigma-Aldrich)], and lysed with glass beads.

For H3K4me3 and H3K56ac ChIP, chromatin was pelleted, washed twice with NP buffer [1.6 M sorbitol, 2 mM $CaCl_2$, 5 mM $MgCl$, 50 mM NaCl, 14 mM β-mercaptoethanol, 10 mM tris-HCl (pH 7.4), 0.075% NP-40, and 5 mM spermidine], resuspended in the same buffer, and digested with MNase (micrococcal nuclease) (9013-53-0, Worthington Biochemical) for 20 min at 37°C, yielding most of the mono- and di-nucleosome fragments. Digestion was stopped with the addition of 5 μl of 0.5 M EDTA and one-fifth volume of 5× ChIP lysis buffer and incubation for 10 min on ice. For RNA Pol II CTD Ser5p ChIP, chromatin was sheared by sonication using Bioruptor Pico (15 s ON, 30 s OFF, 10 cycles) (Diagenode) to yield fragments of an average size of 300 bp.

Sonicated or MNase-digested chromatin was cleared by centrifugation and immunoprecipitated with the appropriate antibody [anti-H3K4me3 (ab8580, Abcam), anti-H3K56ac (*46*), or anti-RPB1 CTD Ser5p (04-1572, Millipore)] and protein G Sepharose beads (17-0618-02, GE Healthcare). After washing the beads extensively, DNA from both input and ChIP was recovered with the Chelex-100 protocol (*47*) and used for BrdU IP/eSPAN or purified with a MinElute PCR Purification kit (28004, Qiagen). ssSeq libraries were prepared using an Accel-NGS 1S Plus DNA library kit (10096, Swift Biosciences).

BrdU IP and eSPAN
Input and ChIP DNA was used for BrdU IP to prepare BrdU IP and eSPAN samples, respectively. Recovered DNA from the Chelex-100 extraction was incubated at 100°C for 5 min and immediately chilled on ice for 5 min. BrdU IP was performed by diluting DNA 10-fold with BrdU IP buffer [phosphate-buffered saline, 0.0625% (v/v) Triton X-100, *Escherichia coli* transfer RNA (6.7 μg/ml), and BrdU antibody (0.17 μg/ml; 555627, BD Biosciences)] and incubated for 2 hours at 4°C. Protein G Sepharose beads were added to each sample for 1 additional hour at 4°C. Beads were washed extensively, and

DNA was recovered with TE (Tris-EDTA buffer) + 1% SDS at 65°C for 15 min and purified with a MinElute PCR Purification kit (28004, Qiagen). ssSeq libraries were prepared using an Accel-NGS 1S Plus DNA library kit (10096, Swift Biosciences).

Protein extracts and immunoblotting

For immunoblotting, 5 ml of each culture was used to prepare protein extracts with trichloroacetic acid, as described previously (48). The following primary antibodies were used for protein detection: anti-H3K4me3 (ab8580, Abcam), anti-H3K56ac (46), anti-H3 (ab1791, Abcam), anti-myc (9E10), anti-HA (12CA5), and anti-AID (S880D, MRC PPU Reagents and Services, UK).

To calculate the H3K4me3/H3 ratio, the indicated strains were exponentially grown for 8 hours at 30°C in YPD. Protein extracts from three biological replicates were serially diluted, immunoblotted, and captured with an Odyssey Fc camera (Li-Cor), and H3K4me3 and H3 signals were measured using ImageJ (49). The H3K4me3:H3 ratio was calculated in WT and mutant strains for each dilution and represented as a proportion of the mutant ratio over the WT ratio.

Cell cycle analysis

For cell cycle analysis, 0.5 ml of yeast culture was harvested by centrifugation at the indicated times, washed with H_2O, and fixed with 70% ethanol. Yeast cells were then washed with 50 mM Na-citrate (pH 7.4), resuspended in the same buffer, and sonicated with three 1-s pulses at 30% amplitude (VCX-500, Sonics Vibra Cell). RNA was degraded with ribonuclease A (0.25 mg/ml; R6513, Sigma-Aldrich) at 50°C for 1 hour, and samples were then treated with proteinase K (1 mg/ml; 25530015, Invitrogen) for 1 hour at 50°C. DNA was stained with propidium iodide (20 μg/ml; P4170, Sigma-Aldrich), and DNA content was analyzed using the Attune Nxt Flow Cytometer (Thermo Fisher Scientific).

Data analysis of ChIP-seq, BrdU-IP-ssSeq, and eSPAN datasets

BrdU-IP-ssSeq, ChIP-seq, and eSPAN libraries were sequenced using the paired-end methods with Illumina NextSeq 500 platforms. Raw reads were trimmed to remove sequencing adaptors using Trim Galore (v0.6.7) (developed by F. Krueger at the Babraham Institute) with default parameters. Reads with an average quality score below 20 and reads shorter than 20 bp after trimming were discarded. Filtered reads were aligned to the *Saccharomyces cerevisiae* reference genome (UCSC sacCer3) using the short reads aligner Bowtie 2 (v2.2.4) (50) with --no-mixed --no-discordant --no-dovetail --no-contain --local parameters. Only paired-end reads with both ends aligning uniquely to the reference genome were used for further analysis after removing multi-mapped reads via SAMtools (v1.11) (51). Reads arising from PCR duplication were removed with Picard (v2.23.8) (Broad Institute). Generated BAM files were converted to Genome Browser visualization files (bigwig format) with score in 1-bp bins using the bamCoverage function from deepTools (v3.2.1) (52).

We determined early-replicated genes (genes that have already been replicated 30 min after release into S phase in the time course in Fig. 1) as follows. MACS2 (v.2.2.5) (53) was used to perform BrdU peak calling (--broad-cutoff 0.001) in the BrdU-IP-ssSeq samples relative to the corresponding control samples (input). Early-replicated regions were determined on the basis of BrdU peaks in the 30 min time point samples (corresponding to early S phase) centered around predefined early-firing replication origins (54). Next, we determined which genes were inside these replicated regions. To eliminate the complications of increased or decreased gene expression on downstream analysis, we selected 640 genes whose expression was not significantly changed between different time points of the cell cycle progression based on the levels of elongating RNA Pol II (RNA Pol II CTD Ser5p ChIP-seq) with the exactTestDoubleTail function from edgeR (55). TSS and termination sites (TTSs) were annotated from the Saccharomyces Genome Database (SGD) (56) and a previous report (57). BEDTools (v2.29.0) (58) coverage function was used for elongating RNA Pol II read counting from TSS to TTS. Reads per kilobase per million reads (RPKM) values for RNA Pol II ChIP-seq were calculated as follows: [(read counts)/(gene length in kb)]/(total uniquely mapped reads in Mb). Metagene ("plotProfile") and heatmap ("plotHeatmap") plots were created using deepTools to display ChIP-seq density.

For BrdU-IP-ssSeq and eSPAN strand bias calculations, consistent paired-end reads mapped to Watson (W) and Crick (C) strands of the reference genome were separated with the bamtobed function from BEDTools and in-house Perl programs. Strand bias was calculated in 10 bp bins from these separated Watson and Crick reads using the formula $Bias = (W - C)/(W + C)$ across the whole genome. Bins with less than 10 sequencing reads were discarded. For eSPAN experiments, strand bias was normalized using the corresponding BrdU-IP-ssSeq strand bias as described previously (54). Strand bias was smoothed by flanking five bins for further visualization. For strand bias analysis on early-replicated genes, bias was calculated as described above but using the whole gene body as a single bin. To calculate the average bias values from all early-replicated genes, the bias of those genes located at the left side of an origin of replication were converted to opposite values so that a leading and lagging bias would correspond to positive and negative values, respectively.

For spike-in normalization, we first followed the same procedure as above to align FASTQ files to the *S. pombe* reference genome (www.pombase.org/ on 10 March 2018). *S. cerevisiae* genome coverage at each base pair was multiplied by a scaling factor based on *S. pombe* reads as described previously (59). Briefly, the scaling factor was calculated as follows: [(*S. pombe* read counts from input sample)/(*S. cerevisiae* read counts from input sample)]/(*S. pombe* read counts from IP sample in Mb). Then, we calculated the H3K4me3 density from 200 bp upstream to 500 bp downstream of the TSS for genes longer than 500 bp, or to the TTS for genes shorter than 500 bp. Last, these densities were multiplied by the scaling factor and then scaled to 1-kb length. To account for differences between sequencing depth among different samples, the *S. pombe*–scaled *S. cerevisiae* read counts were then scaled to 1 million reads. Since our experiments are performed with synchronized *S. cerevisiae* cells over a time course starting at G_1 phase and going through S phase, we would expect the total DNA amount per cell to increase over time. On the other hand, since *S. pombe* cells were not synchronized, the average DNA amount per cell remained constant. Therefore, although we added the same proportion of *S. pombe* cells at each time point based on OD, the proportion of *S. pombe* reads in input samples decreases over the time course. By accounting for input samples in the spike-in normalization calculation of IP samples, we can observe replication-dependent dilution of H3K4me3 in early S phase of the cell cycle.

Define α factor–dependent genes

RNA Pol II Ser5p ChIP-seq read counts of all genes were collected on the basis of the whole gene body (TSS-TTS) using BEDTools (version 2.29.2) (58). Then, differentially expressed genes (DEGs) between G_1 and S phase were identified via edgeR (version 3.34.0) (55) with the cutoff of adjusted P value < 0.05 and fold change > 1.5. Separately, a DEG set between control and 60 nM α-factor treatment was downloaded from GEO (Gene Expression Omnibus) database (GSE8982). We defined 79 α factor–dependent genes by selecting the overlap gene set between DEGs of RNA Pol II Ser5p ChIP-seq and DEGs of the published microarray.

Statistical analysis

All statistical analyses were performed using R software (v3.6.3). Statistical parameters, statistical test used, error bar definitions, and sample sizes are reported in the figures and corresponding figure legends.

SUPPLEMENTARY MATERIALS

Supplementary material for this article is available at https://science.org/doi/10.1126/sciadv.abm6246

View/request a protocol for this paper from *Bio-protocol*.

REFERENCES AND NOTES

1. T. M. Escobar, A. Loyola, D. Reinberg, Parental nucleosome segregation and the inheritance of cellular identity. *Nat. Rev. Genet.* **22**, 379–392 (2021).
2. K. Zhou, G. Gaullier, K. Luger, Nucleosome structure and dynamics are coming of age. *Nat. Struct. Mol. Biol.* **26**, 3–13 (2019).
3. P. B. Talbert, S. Henikoff, The Yin and Yang of histone marks in transcription. *Annu. Rev. Genomics Hum. Genet.* **22**, 147–170 (2021).
4. A. Serra-Cardona, Z. Zhang, Replication-coupled nucleosome assembly in the passage of epigenetic information and cell identity. *Trends Biochem. Sci.* **43**, 136–148 (2018).
5. B. Stillman, Histone modifications: Insights into their influence on gene expression. *Cell* **175**, 6–9 (2018).
6. W. A. Flavahan, E. Gaskell, B. E. Bernstein, Epigenetic plasticity and the hallmarks of cancer. *Science* **357**, eaal2380 (2017).
7. S. P. Bell, A. Dutta, DNA replication in eukaryotic cells. *Annu. Rev. Biochem.* **71**, 333–374 (2002).
8. K. R. Stewart-Morgan, N. Petryk, A. Groth, Chromatin replication and epigenetic cell memory. *Nat. Cell Biol.* **22**, 361–371 (2020).
9. M. Xu, C. Long, X. Chen, C. Huang, S. Chen, B. Zhu, Partitioning of histone H3-H4 tetramers during DNA replication-dependent chromatin assembly. *Science* **328**, 94–98 (2010).
10. G. Schlissel, J. Rine, The nucleosome core particle remembers its position through DNA replication and RNA transcription. *Proc. Natl. Acad. Sci. U.S.A.* **116**, 20605–20611 (2019).
11. T. M. Escobar, O. Oksuz, R. Saldaña-Meyer, N. Descostes, R. Bonasio, D. Reinberg, Active and repressed chromatin domains exhibit distinct nucleosome segregation during dna replication. *Cell* **179**, 953–963.e11 (2019).
12. R. Margueron, N. Justin, K. Ohno, M. L. Sharpe, J. Son, W. J. Drury 3rd, P. Voigt, S. R. Martin, W. R. Taylor, V. De Marco, V. Pirrotta, D. Reinberg, S. J. Gamblin, Role of the polycomb protein EED in the propagation of repressive histone marks. *Nature* **461**, 762–767 (2009).
13. K. Ragunathan, G. Jih, D. Moazed, Epigenetic inheritance uncoupled from sequence-specific recruitment. *Science* **348**, 1258699 (2015).
14. N. Liu, Z. Zhang, H. Wu, Y. Jiang, L. Meng, J. Xiong, Z. Zhao, X. Zhou, J. Li, H. Li, Y. Zheng, S. Chen, T. Cai, S. Gao, B. Zhu, Recognition of H3K9 methylation by GLP is required for efficient establishment of H3K9 methylation, rapid target gene repression, and mouse viability. *Genes Dev.* **29**, 379–393 (2015).
15. D. Reinberg, L. D. Vales, Chromatin domains rich in inheritance. *Science* **361**, 33–34 (2018).
16. A. J. Ruthenburg, W. Wang, D. M. Graybosch, H. Li, C. D. Allis, D. J. Patel, G. L. Verdine, Histone H3 recognition and presentation by the WDR5 module of the MLL1 complex. *Nat. Struct. Mol. Biol.* **13**, 704–712 (2006).
17. J. Wysocka, T. Swigut, T. A. Milne, Y. Dou, X. Zhang, A. L. Burlingame, R. G. Roeder, A. H. Brivanlou, C. D. Allis, WDR5 associates with histone H3 methylated at K4 and is essential for H3 K4 methylation and vertebrate development. *Cell* **121**, 859–872 (2005).
18. C. Yu, H. Gan, A. Serra-Cardona, L. Zhang, S. Gan, S. Sharma, E. Johansson, A. Chabes, R.-M. Xu, Z. Zhang, A mechanism for preventing asymmetric histone segregation onto replicating DNA strands. *Science* **361**, 1386–1389 (2018).

19. N. Petryk, M. Dalby, A. Wenger, C. B. Stromme, A. Strandsby, R. Andersson, A. Groth, MCM2 promotes symmetric inheritance of modified histones during DNA replication. *Science* **361**, 1389–1392 (2018).
20. M. Wooten, R. Ranjan, X. Chen, Asymmetric histone inheritance in asymmetrically dividing stem cells. *Trends Genet.* **36**, 30–43 (2020).
21. H. Gan, A. Serra-Cardona, X. Hua, H. Zhou, K. Labib, C. Yu, Z. Zhang, The Mcm2-Ctf4-polα axis facilitates parental histone H3-H4 transfer to lagging strands. *Mol. Cell* **72**, 140–151.e3 (2018).
22. Z. Li, X. Hua, A. Serra-Cardona, X. Xu, S. Gan, H. Zhou, W.-S. Yang, C.-I. Chen, R.-M. Xu, Z. Zhang, DNA polymerase α interacts with H3-H4 and facilitates the transfer of parental histones to lagging strands. *Sci. Adv.* **6**, eabb5820 (2020).
23. M. Foltman, C. Evrin, G. De Piccoli, R. C. Jones, R. D. Edmondson, Y. Katou, R. Nakato, K. Shirahige, K. Labib, Eukaryotic replisome components cooperate to process histones during chromosome replication. *Cell Rep.* **3**, 892–904 (2013).
24. A. Shilatifard, The COMPASS family of histone H3K4 methylases: Mechanisms of regulation in development and disease pathogenesis. *Annu. Rev. Biochem.* **81**, 65–95 (2012).
25. H. Masumoto, D. Hawke, R. Kobayashi, A. Verreault, A role for cell-cycle-regulated histone H3 lysine 56 acetylation in the DNA damage response. *Nature* **436**, 294–298 (2005).
26. A. Marie-Josee Sasseville, A. W. Caron, L. Bourget, A. F. Klein, M. J. Dicaire, G. A. Rouleau, B. Massie, Y. Langelier, B. Brais, The dynamism of PABPN1 nuclear inclusions during the cell cycle. *Neurobiol. Dis.* **23**, 621–629 (2006).
27. C. He, N. Liu, D. Xie, Y. Liu, Y. Xiao, F. Li, Structural basis for histone H3K4me3 recognition by the N-terminal domain of the PHD finger protein Spp1. *Biochem. J.* **476**, 1957–1973 (2019).
28. C. Adam, R. Guerois, A. Citarella, L. Verardi, F. Adolphe, C. Beneut, V. Sommermeyer, C. Ramus, J. Govin, Y. Coute, V. Borde, The PHD finger protein Spp1 has distinct functions in the Set1 and the meiotic DSB formation complexes. *PLOS Genet.* **14**, e1007223 (2018).
29. Z. Karanyi, L. Halasz, L. Acquaviva, D. Jonas, S. Hetey, B. Boros-Olah, F. Peng, D. Chen, F. Klein, V. Geli, L. Szekvolgyi, Nuclear dynamics of the Set1C subunit Spp1 prepares meiotic recombination sites for break formation. *J. Cell Biol.* **217**, 3398–3415 (2018).
30. L. Acquaviva, L. Szekvolgyi, B. Dichtl, B. S. Dichtl, C. de La Roche Saint Andre, A. Nicolas, V. Geli, The COMPASS subunit Spp1 links histone methylation to initiation of meiotic recombination. *Science* **339**, 215–218 (2013).
31. V. Sommermeyer, C. Béneut, E. Chaplais, M. E. Serrentino, V. Borde, Spp1, a member of the Set1 complex, promotes meiotic DSB formation in promoters by tethering histone H3K4 methylation sites to chromosome axes. *Mol. Cell* **49**, 43–54 (2013).
32. N. Reveron-Gomez, C. Gonzalez-Aguilera, K. R. Stewart-Morgan, N. Petryk, V. Flury, S. Graziano, J. V. Johansen, J. S. Jakobsen, C. Alabert, A. Groth, Accurate recycling of parental histones reproduces the histone modification landscape during DNA replication. *Mol. Cell* **72**, 239–249.e5 (2018).
33. S. Battaglia, M. Lidschreiber, C. Baejen, P. Torkler, S. M. Vos, P. Cramer, RNA-dependent chromatin association of transcription elongation factors and Pol II CTD kinases. *eLife* **6**, e25637 (2017).
34. C. Alabert, T. K. Barth, N. Reveron-Gomez, S. Sidoli, A. Schmidt, O. N. Jensen, A. Imhof, A. Groth, Two distinct modes for propagation of histone PTMs across the cell cycle. *Genes Dev.* **29**, 585–590 (2015).
35. H. J. Bae, M. Dubarry, J. Jeon, L. M. Soares, C. Dargemont, J. Kim, V. Geli, S. Buratowski, The Set1 N-terminal domain and Swd2 interact with RNA polymerase II CTD to recruit COMPASS. *Nat. Commun.* **11**, 2181 (2020).
36. B. E. Bernstein, T. S. Mikkelsen, X. Xie, M. Kamal, D. J. Huebert, J. Cuff, B. Fry, A. Meissner, M. Wernig, K. Plath, R. Jaenisch, A. Wagschal, R. Feil, S. L. Schreiber, E. S. Lander, A bivalent chromatin structure marks key developmental genes in embryonic stem cells. *Cell* **125**, 315–326 (2006).
37. J. A. Dahl, I. Jung, H. Aanes, G. D. Greggains, A. Manaf, M. Lerdrup, G. Li, S. Kuan, B. Li, A. Y. Lee, S. Preissl, I. Jermstad, M. H. Haugen, R. Suganthan, M. Bjoras, K. Hansen, K. T. Dalen, P. Fedorcsak, B. Ren, A. Klungland, Broad histone H3K4me3 domains in mouse oocytes modulate maternal-to-zygotic transition. *Nature* **537**, 548–552 (2016).
38. B. Zhang, H. Zheng, B. Huang, W. Li, Y. Xiang, X. Peng, J. Ming, X. Wu, Y. Zhang, Q. Xu, W. Liu, X. Kou, Y. Zhao, W. He, C. Li, B. Chen, Y. Li, Q. Wang, J. Ma, Q. Yin, K. Kee, A. Meng, S. Gao, F. Xu, J. Na, W. Xie, Allelic reprogramming of the histone modification H3K4me3 in early mammalian development. *Nature* **537**, 553–557 (2016).
39. R. K. Ng, J. B. Gurdon, Epigenetic memory of an active gene state depends on histone H3.3 incorporation into chromatin in the absence of transcription. *Nat. Cell Biol.* **10**, 102–109 (2008).
40. E. Hormanseder, A. Simeone, G. E. Allen, C. R. Bradshaw, M. Figlmuller, J. Gurdon, J. Jullien, H3K4 methylation-dependent memory of somatic cell identity inhibits reprogramming and development of nuclear transfer embryos. *Cell Stem Cell* **21**, 135–143.e6 (2017).

41. E. L. Greer, T. J. Maures, D. Ucar, A. G. Hauswirth, E. Mancini, J. P. Lim, B. A. Benayoun, Y. Shi, A. Brunet, Transgenerational epigenetic inheritance of longevity in Caenorhabditis elegans. *Nature* **479**, 365–371 (2011).

42. B. E. Collins, C. B. Greer, B. C. Coleman, J. D. Sweatt, Histone H3 lysine K4 methylation and its role in learning and memory. *Epigenetics Chromatin* **12**, 7 (2019).

43. C. Noguchi, M. V. Garabedian, M. Malik, E. Noguchi, A vector system for genomic FLAG epitope-tagging in Schizosaccharomyces pombe. *Biotechnol. J.* **3**, 1280–1285 (2008).

44. M. F. Laughery, T. Hunter, A. Brown, J. Hoopes, T. Ostbye, T. Shumaker, J. J. Wyrick, New vectors for simple and streamlined CRISPR-Cas9 genome editing in Saccharomyces cerevisiae. *Yeast* **32**, 711–720 (2015).

45. D. Mumberg, R. Muller, M. Funk, Regulatable promoters of Saccharomyces cerevisiae: Comparison of transcriptional activity and their use for heterologous expression. *Nucleic Acids Res.* **22**, 5767–5768 (1994).

46. J. Han, H. Zhou, B. Horazdovsky, K. Zhang, R. M. Xu, Z. Zhang, Rtt109 acetylates histone H3 lysine 56 and functions in DNA replication. *Science* **315**, 653–655 (2007).

47. J. D. Nelson, O. Denisenko, K. Bomsztyk, Protocol for the fast chromatin immunoprecipitation (ChIP) method. *Nat. Protoc.* **1**, 179–185 (2006).

48. M. Foiani, F. Marini, D. Gamba, G. Lucchini, P. Plevani, The B subunit of the DNA polymerase alpha-primase complex in Saccharomyces cerevisiae executes an essential function at the initial stage of DNA replication. *Mol. Cell. Biol.* **14**, 923–933 (1994).

49. C. A. Schneider, W. S. Rasband, K. W. Eliceiri, NIH Image to ImageJ: 25 years of image analysis. *Nat. Methods* **9**, 671–675 (2012).

50. B. Langmead, S. L. Salzberg, Fast gapped-read alignment with Bowtie 2. *Nat. Methods* **9**, 357–359 (2012).

51. P. Danecek, J. K. Bonfield, J. Liddle, J. Marshall, V. Ohan, M. O. Pollard, A. Whitwham, T. Keane, S. A. McCarthy, R. M. Davies, H. Li, Twelve years of SAMtools and BCFtools. *Gigascience* **10**, 1–4 (2021).

52. F. Ramirez, D. P. Ryan, B. Gruning, V. Bhardwaj, F. Kilpert, A. S. Richter, S. Heyne, F. Dundar, T. Manke, deepTools2: A next generation web server for deep-sequencing data analysis. *Nucleic Acids Res.* **44**, W160–W165 (2016).

53. J. X. Feng, T. Liu, B. Qin, Y. Zhang, X. S. Liu, Identifying ChIP-seq enrichment using MACS. *Nat. Protoc.* **7**, 1728–1740 (2012).

54. C. Yu, H. Gan, J. Han, Z. X. Zhou, S. Jia, A. Chabes, G. Farrugia, T. Ordog, Z. Zhang, Strand-specific analysis shows protein binding at replication forks and PCNA unloading from lagging strands when forks stall. *Mol. Cell* **56**, 551–563 (2014).

55. D. J. McCarthy, Y. S. Chen, G. K. Smyth, Differential expression analysis of multifactor RNA-Seq experiments with respect to biological variation. *Nucleic Acids Res.* **40**, 4288–4297 (2012).

56. U. Nagalakshmi, Z. Wang, K. Waern, C. Shou, D. Raha, M. Gerstein, M. Snyder, The transcriptional landscape of the yeast genome defined by RNA sequencing. *Science* **320**, 1344–1349 (2008).

57. Z. Y. Xu, W. Wei, J. Gagneur, F. Perocchi, S. Clauder-Munster, J. Camblong, E. Guffanti, F. Stutz, W. Huber, L. M. Steinmetz, Bidirectional promoters generate pervasive transcription in yeast. *Nature* **457**, 1033–1037 (2009).

58. A. R. Quinlan, I. M. Hall, BEDTools: A flexible suite of utilities for comparing genomic features. *Bioinformatics* **26**, 841–842 (2010).

59. C. Jeronimo, C. Poitras, F. Robert, Histone recycling by FACT and Spt6 during transcription prevents the scrambling of histone modifications. *Cell Rep.* **28**, 1206–1218.e8 (2019).